High-level direct-dynamics variational transition state theory calculations including multidimensional tunneling of the thermal rate constants, branching ratios, and kinetic isotope effects of the hydrogen abstraction reactions from methanol by atomic hydrogen

Rubén Meana-Pañeda,[1] Donald G. Truhlar,[2] and Antonio Fernández-Ramos[1,a)]
[1]*Department of Physical Chemistry and Center for Research in Biological Chemistry and Molecular Materials, University of Santiago de Compostela, 15706 Santiago de Compostela, Spain*
[2]*Department of Chemistry and Supercomputing Institute, University of Minnesota, 207 Pleasant Street S. E., Minneapolis, Minnesota 55455-0431, USA*

(Received 25 October 2010; accepted 28 January 2011; published online 2 March 2011)

We report a detailed theoretical study of the hydrogen abstraction reaction from methanol by atomic hydrogen. The study includes the analysis of thermal rate constants, branching ratios, and kinetic isotope effects. Specifically, we have performed high-level computations at the MC3BB level together with direct dynamics calculations by canonical variational transition state theory (CVT) with the microcanonically optimized multidimensional tunneling (μOMT) transmission coefficient (CVT/μOMT) to study both the $CH_3OH + H \rightarrow CH_2OH + H_2$ (R1) reaction and the $CH_3OH + H \rightarrow CH_3O + H_2$ (R2) reaction. The CVT/μOMT calculations show that reaction R1 dominates in the whole range $298 \leq T(K) \leq 2500$ and that anharmonic effects on the torsional mode about the C–O bond are important, mainly at high temperatures. The activation energy for the total reaction sum of R1 and R2 reactions changes substantially with temperature and, therefore, the use of straight-line Arrhenius plots is not valid. We recommend the use of new expressions for the total R1 + R2 reaction and for the R1 and R2 individual reactions. © *2011 American Institute of Physics*. [doi:10.1063/1.3555763]

I. INTRODUCTION

The combustion of methanol is a complex process which is not completely understood,[1–13] although the importance of the H and OH radicals in the early stages of the combustion is well established; these radicals are formed mainly from unimolecular decomposition of methanol.[11,14–16] For instance, the hydrogen abstraction reaction by atomic hydrogen consumes a significant fraction of the methanol, particularly under fuel-rich conditions,[5] through the reactions:

$$CH_3OH + H \rightarrow CH_2OH + H_2 \quad \text{(R1)}$$

$$CH_3OH + H \rightarrow CH_3O + H. \quad \text{(R2)}$$

There is a third possible reaction, which could compete with the R1 and R2 hydrogen abstraction reactions, that leads to the formation of methyl radicals:

$$CH_3OH + H \rightarrow CH_3 + H_2O. \quad \text{(R3)}$$

However, the experiments on the pyrolysis of methanol carried out by Aronowitz *et al.*[17] in the temperature range 1070–1225 K and the discharge flow reactor experiments carried out by Hoyermann *et al.*[18] between 500 and 680 K indicate that the disappearance of methanol through this channel is only minor. This aspect has also been confirmed by theoretical calculations.[19]

Reactions R1 and R2 involve the formation of the hydroxymethyl CH_2OH and methoxy CH_3O radicals, respectively. The formation of these two radicals and the ratio between their concentrations is of great importance in the combustion of methanol because the two species are isomers that have different reactivities. Direct measurements of the total hydrogen abstraction (R1 + R2) thermal rate constants were carried out by Aders and Wagner,[20] Meagher *et al.*,[21] and Hoyermann *et al.*[18] These experiments were performed in the temperature range $T = 295$–680 K. At higher temperatures (between $T = 1000$ and 2740 K), the total abstraction rate constants were obtained from lean methanol flames[14] and from the pyrolysis of methanol[16]—in both cases the measurement of the thermal rate constants is complicated by side reactions. There is a significant discrepancy between the low-temperature experiments, which yield activation energies about 5.4 kcal/mol, and the high-temperature activation energies reported by Vandooren and Tiggelen[14] and by Cribb *et al.*[16] with values of 2.6 and 14.1 kcal/mol, respectively. Tsang[22] gave a recommended expression in the temperature range of $T = 600$–2000 K using bond-order bond-energy (BEBO) transition state calculations to fit the low-temperature experiments and those of Vandooren and Tiggelen.[14] To our knowledge, the latest review on the R1 + R2 hydrogen abstraction reactions was carried out by Baulch *et al.*,[23] who disregarded the low-temperature data of Meagher *et al.*[21] obtained by electron spin resonance (ESR) and used the mean value of the results of Vandooren and Tiggelen[14] and Cribb *et al.*[16] at $T = 2000$ K. The recommended expressions

a)Electronic mail: qf.ramos@usc.es.

reported by Tsang[22] and by Baulch *et al.*[23] give similar results at about $T = 600$ K, but they disagree by more than a factor of 4 at $T = 2000$ K, as a consequence of including different experimental results in their fits at high temperatures.

Another aspect about which there is very little information is the branching ratio between R1 and R2 because the above experiments do not distinguish between the two reactions. For instance, Held and Dryer[7] indicated that reaction R1 dominates at low temperatures and that the ratio of the two reaction rate constants does not change with temperature. Tsang,[22] using experimental data on methyl attack on methanol, recommended a k_{R1}/k_{R2} value of 4 with an uncertainty factor of 3, where k_{R1} and k_{R2} are the thermal rate constants of reactions R1 and R2, respectively. Li and Williams[10] gave a temperature-dependent expression for the ratio k_{R1}/k_{R2} constants, but the accuracy of their result is difficult to assess, since it is based on a methanol combustion mechanism that involves 92 elementary reactions.

As indicated above, both the values of the thermal rate constants for the hydrogen abstraction reactions from methanol and the branching ratios are uncertain mainly due to the large number of side reactions that must be considered. In cases like this, theoretical calculations can be useful. Several authors have carried out electronic structure calculations at various levels of theory[19,24–32] and have computed thermal rate constants.[19,26–29,32] We are concerned here only with gas-phase studies. The thermal rate constant obtained by Lendvay *et al.*[19] and Jodkowski *et al.*[26] were calculated by combining conventional transition state theory[33] with one-dimensional tunneling corrections (Wigner correction[34] in Ref. 19 and Eckart barrier correction[35] in Ref. 26). Carvalho *et al.*[32] performed zero-order interpolated variational transition state[36] with zero-curvature tunneling[37] (ZCT) corrections for tunneling. Kerkeni and Clary[28] applied a two-dimensional reduced dimensionality quantum dynamics model to reactions R1 and R2 and pointed out the importance of including quantum effects for both reactions. In this context, it should be noticed that both the one-dimensional and the ZCT models for tunneling seriously underestimate those quantum effects,[38–42] so an approach based on multidimensional tunneling paths is needed.

Variational transition state theory[43–47] with multidimensional corrections for tunneling[39,42,47–53] (VTST/MT) can yield accurate thermal rate constants[41,54] for reactions with important quantum effects. It can also account for recrossing effects, so, the accuracy of the VTST/MT results depends largely on the accuracy of the potential energy surface. For the hydrogen abstraction reaction R1, VTST/MT calculations have been carried previously by Chuang *et al.*,[27] but the results were handicapped by the low accuracy of the electronic structure calculations, which yield a gas-phase classical barrier height of 7.8 kcal/mol, which differs considerably from benchmark calculations performed at the W1RO level[55] that lead to a classical barrier height of 9.6 kcal/mol[56] and from a later estimate of 9.7 kcal/mol.[30]

Nowadays, it is possible to use VTST/MT together with electronic structure calculations that are very close to chemical accuracy. In this context, it is the main goal of this work to provide reliable thermal rate constants for reactions R1 and R2, so in the first place we perform electronic structure calculations at one of the most accurate levels for reaction R1, as suggested in a comprehensive examination[30] of R1, and in the second place, we apply VTST/MT.

Another aspect of interest, which may help to identify the main channel for hydrogen abstraction, is the evaluation of the kinetic isotope effects (KIEs). Meagher *et al.*[21] have reported experimental thermal rate constants for the reaction,

$$CH_3OH + D \rightarrow CH_2OH + HD \quad \text{(R4)}$$

in the temperature range $298 \leq T(\mathrm{K}) \leq 575$.

Hoyermann *et al.*,[18] in the temperature range $500 \leq T(\mathrm{K}) \leq 680$, prepared deuterated methanol and reported values of the thermal rate constants for the reactions,

$$CD_3OD + H \rightarrow CD_2OD + HD, \quad \text{(R5)}$$

$$CD_3OH + H \rightarrow CD_2OH + HD. \quad \text{(R6)}$$

In the analysis of the products of reactions R5 and R6 those authors detected the presence of CD_2O, CDOH, and CD_2HOH radicals, which can be obtained by fast reactions of the radicals CD_2OD and CD_2OH with atomic hydrogen. The products CDOH and CD_2HOH can only be obtained from hydrogen abstraction reactions from the methyl group, whereas the CD_2O radical can also be obtained from the methoxy radical. Therefore, they could not unambiguously conclude that reaction R1 dominates at those temperatures.

From the theoretical point of view, the detailed analysis of KIEs can bring additional information about the role played by quantum effects on these systems, so we include reactions R4 and R5 in the present VTST/MT study.

II. METHODOLOGY

In this section, we first describe the method used to carry out the electronic structure calculations to build the potential energy surface, and after that, we briefly describe canonical variational transition state theory with multidimensional tunneling corrections.

II.A. Electronic structure

Benchmark calculations of reaction energies, barrier heights, and transition state geometries for reaction R1 were reported by Pu and Truhlar.[30] Those authors classified the methods by their asymptotic computational scaling behaviors N^α (where N is the number of atoms and α is a parameter in the range 3–7), obtaining, for reaction R1, a consensus value from the N^7 methods for the forward barrier and reaction energy of 9.7 and −6.3 kcal/mol, respectively. These values are very close to those obtained at the W1RO and W1BD levels which lead to values of 9.6 kcal/mol for the barrier height and −6.1 and −6.0 kcal/mol, respectively, for the reaction energy, as shown in Table I. In this work, we use one of the methods that Pu and Truhlar[30] recommend for high-level dynamics calculations, i.e., the multicoefficient three-parameters Becke88–Becke95 (MC3BB) method,[57] which yields a barrier height of 9.8 kcal/mol. This method also gives a very

TABLE I. Energetic parameters (in kcal/mol) of reactions R1 and R2 obtained at different levels of theory. $V^{\ddagger}$ is the barrier height, ΔE is the classical energy of reaction, $\Delta H_0^{\ddagger,o}$ is the conventional transition state theory enthalpy of activation at 0 K, and ΔH_0^o is the enthalpy of reaction at 0 K. Experimental values are also listed for comparison.

Method	$V^{\ddagger}$	ΔE	$\Delta H_0^{\ddagger,o}$	ΔH_0^o	Reference
			R1		
Estimate	9.7	–6.3	…	…	30
W1RO	9.6	–6.1	8.2	–8.5	55
W1BD	9.6	–6.0	8.2	–8.4	This work
MC3BB	9.8	–4.7	8.4	–7.2	30
G2	10.6	–5.6	9.0	–8.2	19 and 26
CCSD(T,full)//MP2(full)/cc-pVTZ	9.9	–5.5	8.6	–7.9	28
CCSD(T,full)/cc-pVTZ	9.8	–6.1	7.8	–8.5	32
Exp.	…	…	…	–8.8 ±0.4	58
			R2		
W1RO	15.3	3.7	13.3	0.7	This work
W1BD	15.2	3.7	13.3	0.6	This work
MC3BB	15.6	3.8	13.7	0.8	This work
G2	16.3	3.1	14.2	0.6	19 and 26
CCSD(T)//MP2(full)/cc-pVTZ	14.9	2.8	13.3	0.2	28
CCSD(T,full)/cc-pVTZ	14.8	2.3	12.7	–0.7	32
Exp.	…	…	…	–0.3 ±1.0	58

similar reaction energetics to the W1R0 and W1BD methods for reaction R2. The experimental enthalpies of reaction[58] show that reaction R1 is exothermic whereas reaction R2 is almost thermoneutral (although most of the theoretical methods listed in Table I predict a slight endothermicity). The CCSD(T,full)//MP2(full)/cc-pVTZ and CCSD(T,full)/cc-pVTZ method gives similar results to the MC3BB methods, but the latter is more suitable for dynamical calculations because it scales as N^5, whereas CCSD(T, full) methods scale as N^7. On the other hand, the G2 calculations carried out by Lendvay *et al.*[19] and by Jodkowski *et al.*,[26] which also scale as N^7, yield to reaction barrier heights that are probably too high by more than 0.5 kcal/mol.

The MC3BB method merges scaling-all-correlation theory[59] with a modification of the Becke88–Becke95[60,61] one-parameter model for kinetics[62] (BB1K) with empirical parameters to make the method more accurate than other methods scaling as N^5. The MC3BB energy is obtained by the expression,

$$E(\text{MC3BB}) = c_2[E(\text{HF/DIDZ}) + c_1\Delta E(\text{MP2|HF/DIDZ})] + (1 - c_2)E(\text{BB}X/\text{MG3S}), \quad (1)$$

where the empirical coefficients c_1 and c_2 are equal to 1.332 and 0.205, respectively; BBX is the same as BB1K except that the percentage of Hartree–Fock exchange is 39% instead of 42%; DIDZ refers to the 6-31+G(d,p) basis set,[63] and MG3S is a minimally augmented polarized triple-ζ basis set.[64]

II.B. Reaction rates

The thermal rate constants for the hydrogen abstraction reactions from methanol were calculated by means of canonical variational transition-state theory with a multidimensional treatment of tunneling (CVT/MT).[46,65] All the electronic structure calculations were performed at the MC3BB level using a direct dynamics approach,[66] i.e., the points to build the potential energy surface needed for the dynamics were calculated "on the fly." The canonical variational version of transition state theory implies that the reactants are equilibrated canonically (in a fixed-temperature ensemble) and that the transition state dividing surface (the bottleneck for reaction) minimizes the one-way flux toward products by passing through the point on the minimum energy path[37,67,68] (MEP) that presents a maximum in the generalized free energy of activation.[46,69,70]

The MEP is the union of the paths of steepest descent in isoinertial coordinates from the saddle point to the reactants and to the products, and the signed distance along this path is labeled as s. The MEP was followed in mass-scaled Cartesian coordinates (mass-weighted Cartesian coordinates divided by the square root of an arbitrary scaling mass μ) by the Page–McIver method[71] using a stepsize of 0.005 a_0 and a scaling mass $\mu = 1$, and Hessians were calculated each nine steps. All the harmonic vibrational frequencies along the MEP were obtained using redundant internal coordinates[72] and scaled by a factor of 0.9669.[57] The CVT/MT expression to evaluate thermal rate constants, $k^{\text{CVT/X}}$, at a given temperature, T, is given by

$$k^{\text{CVT}/X}(T) = \kappa^{\text{CVT}/X}k^{\text{CVT}}(T), \quad (2)$$

where $\kappa^{\text{CVT/X}}$ is the ground-state transmission coefficient computed with the multidimensional method X, and $k^{\text{CVT}}(T)$ is the quasiclassical canonical thermal rate constant

$$k^{\text{CVT}}(T) = \min_s k^{\text{GT}}(T, s) = \sigma\frac{1}{\beta h}\frac{Q^{\text{GT}}(T, s_*^{\text{CVT}})}{\Phi_{\text{R}}(T)}\exp\left[-\beta V_{\text{MEP}}(s_*^{\text{CVT}})\right], \quad (3)$$

where k_{B} is the Boltzmann constant; h is the Planck constant; σ is the symmetry number;[73,74] $V_{\text{MEP}}\left(s_*^{\text{CVT}}\right)$ is the classical potential at point s_*^{CVT} of the MEP. The value s_*^{CVT} is

chosen as the point of the MEP in which the free energy of activation has a maximum, or similarly, as the generalized transition (GT) at which is located the bottleneck for reaction. $Q^{\mathrm{GT}}(T, s_*^{\mathrm{CVT}})$ is the product of the rotational, vibrational, and electronic partition functions of the generalized transition state. Here, $\Phi_{\mathrm{R}}(T)$ is the partition function of reactants per unit volume and is given as the product of the partition functions for the two reactant species and their relative translational motion. Note that we omit symmetry numbers from rotational partition functions and instead accumulate these in an overall symmetry number σ, as discussed further below.

The term "quasiclassical" means that, except for the reaction coordinate, which corresponds to the mode with imaginary frequency at the transition state, all the remaining $3N - 7$ vibrational modes ($3N - 6$ modes for linear molecules; N being the number of atoms) are treated quantally by using quantum vibrational partition functions in the rate constant expression of Eq. (3). Quantum mechanical effects on the reaction-coordinate motion are incorporated by the ground-state transmission coefficient,[47,75] which multiplies the rate constant of Eq. (2) and is given by

$$\kappa^{\mathrm{CVT}/X}(T) = \kappa^{\mathrm{CVT/CAG}}\kappa^{X}, \tag{4}$$

where $\kappa^{\mathrm{CVT/CAG}}$ corrects for the different thresholds which may have the CVT thermal rate constant and the tunneling transmission coefficient κ^{X}.[75] For reactions with tight transition states, such as reactions R1 and R2, $\kappa^{\mathrm{CVT/CAG}}$ is usually very close, within 5%, to unity. The tunneling transmission coefficient κ^{X} is given by

$$\kappa^{X}(T) = \beta \exp\left(\beta V_{\mathrm{a}}^{\mathrm{AG}}\right) \int_{E_0}^{\infty} dE\, P^{X}(E) \exp(-\beta E), \tag{5}$$

where $P^{X}(E)$ is the semiclassical ground-state reaction probability computed by approximation X. The lower limit of the integral is the lowest energy at which it is possible to have tunneling, i.e., it is the energy of the reactant zero-point level when the reaction is written in the exoergic direction; $V_{\mathrm{a}}^{\mathrm{AG}}$ is the maximum of the vibrationally adiabatic potential which is given by

$$V_{\mathrm{a}}^{\mathrm{G}}(s) = V_{\mathrm{MEP}}(s) + \epsilon_{\mathrm{int}}^{G}(s), \tag{6}$$

where $\epsilon_{\mathrm{int}}^{\mathrm{G}}(s)$ denotes the zero-point energy (ZPE) of the vibrational modes transverse to the MEP.

In the present work, the semiclassical probability $P^{X}(E)$ at every tunneling energy E has been calculated by the microcanonically optimized multidimensional tunneling (μOMT) approximation,[76] which chooses the largest value between the small-curvature tunneling[77–80] (SCT) probability, $P^{\mathrm{SCT}}(E)$, and the large-curvature tunneling[50,53,76,79,81–85] (LCT) probability $P^{\mathrm{LCT}}(E)$; the latter being evaluated with the version 4 of the LCT method,[85]

$$P^{\mu\mathrm{OMT}} = \max_{E} \begin{cases} P^{\mathrm{SCT}}(E) \\ P^{\mathrm{LCT}}(E). \end{cases} \tag{7}$$

The LCT tunneling probabilities were evaluated using the interpolated large-curvature tunneling in two dimensions[86] (ILCT2D) algorithm. The electronic structure calculations were performed with GAUSSIAN03,[87] the thermal rate constants CVT/μOMT were calculated with version 9.7 of the POLYRATE program.[88] A modified version of the GAUSSRATE9.7[89] program made the linkage between the two packages. Some of the data shown in Sec. III were extracted from graphs made by the WINDIG program,[90] i.e., from: Fig. 4 of Ref. 18, Fig. 13 of Ref. 28, and Fig. 3 of Ref. 29.

III. RESULTS AND DISCUSSION

In this section, we first describe some important issues related to the stationary points of the hydrogen abstraction reaction, which includes the anharmonic treatment of the torsional mode about the C–O bond, then we discuss the CVT/μOMT calculations carried out in this work, initially in the context of previous theoretical calculations and second in the context of the experiment. Finally, we discuss the results obtained in this work for the branching ratios and KIEs.

III.A. Stationary points

All electronic structure calculations needed for the dynamics calculations were carried out at MC3BB level.[57] The optimized geometries of the stationary points are shown in Fig. 1. The equilibrium configuration of methanol has C_s point-group symmetry. The hydrogen atom can be abstracted from the CH_3 group or from the OH group, forming the hydroxymethyl radical (reaction R1) or the methoxy radical (reaction R2) from the transition states TS-R1 and TS-R2, respectively. For reaction R1, the hydrogen atom from the methyl group is abstracted in a *gauche* conformation, forming a dihedral angle with the hydrogen atom of the hydroxyl of 74°. This transition state is chiral and, therefore, it has one enantiomer. The interconversion between enantiomers is possible by rotation about the C−O bond. The top of the rotational barrier is a second-order saddle point and corresponds to the eclipsed conformation. The calculated barrier height at the MC3BB has a value of 2.9 kcal/mol with respect to the saddle point energy. The interconversion is also possible through a second-order saddle point corresponding to an anticonformation, but in this case the barrier is higher, i.e.,

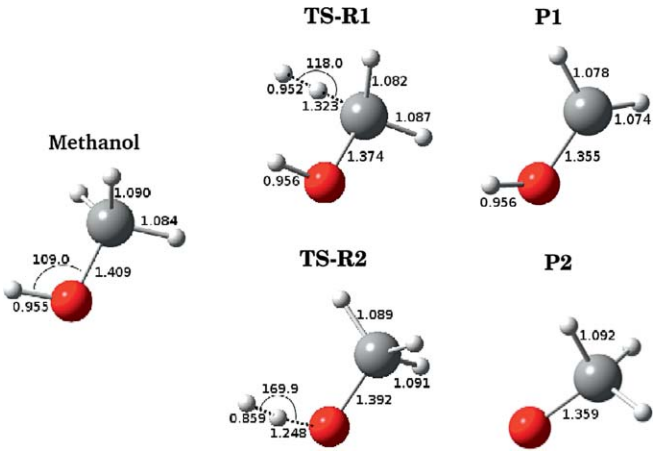

FIG. 1. Geometries of the stationary points for reactions R1 and R2. TS-R1 and TS-R2 are the transition state geometries for reactions R1 and R2, respectively. Distances are in Å; bond and dihedral angles are in degrees.

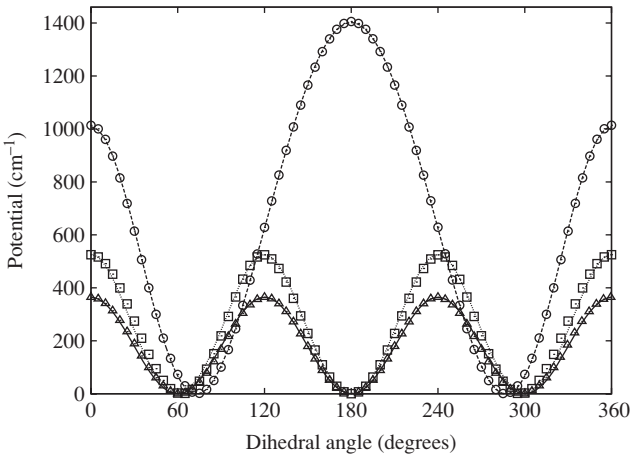

FIG. 2. Torsional potentials (in cm^{-1}) calculated at the MC3BB level about the C–O bond for methanol (triangles), TS-R1 (circles), and TS-R2 (squares). The potentials were fitted to cosine Fourier series given by Eqs. (12), (13), and (14) and shown in the plot as solid line, dashed line, and dotted line for methanol, TS-R1 and TS-R2, respectively.

4.0 kcal/mol. Chuang *et al.*[27] using a semiempirical method obtained similar barriers of 3.3 and 4.2 kcal/mol for the eclipsed and *anti* conformations. Those authors pointed out that the barriers between transition states (which are the minima along the torsion coordinate) are high enough, so they can be treated as two independent reactive channels.

Several theoretical works[26,28,32] ignored the chiral nature of the transition state and pointed out that for reaction R1 because methanol has three reactive hydrogens, the symmetry number entering the transition state theory expression [same as Eq. (3) but with the dividing surface located at the transition state] should be 3. It should be noticed that the symmetry number is given by[73,74]

$$\sigma = \frac{\sigma_{\mathrm{R}} n_{\mathrm{TS}}}{\sigma_{\mathrm{TS}} n_{\mathrm{R}}}, \tag{8}$$

where n_{TS} and n_{R} are the number of enantiomers of the transition state and the reactants, respectively; σ_{R} and σ_{TS} are the symmetry numbers of the rotational partition function of the reactants and the transition state, respectively. Taking into account that the minimum-energy configuration of methanol belongs to the C_s point-group symmetry (so $\sigma_{\mathrm{R}} = 1$) and that the transition state has two enantiomers, the symmetry number for reaction R1 is 2. To our knowledge, this issue was only correctly addressed by Chuang *et al.*[27]. Hereafter, all the theoretical rate constants that included a factor of 3 (Refs. 26,28, and 32) were multiplied by 2/3 to correct the symmetry number.

For reaction R2 the symmetry number is the unity.

III.B. Anharmonicity

The previous theoretical works[26–28,32] have treated the torsional motion of the methyl group of methanol as a harmonic-oscillator (HO) vibration, i.e., the partition function, $Q_{\mathrm{tor}}^{\mathrm{HO,CH_3OH}}$, of this normal mode is given by

$$Q_{\mathrm{tor}}^{\mathrm{HO,CH_3OH}} = \frac{e^{-\beta\hbar\omega_{\mathrm{tor}}^{\mathrm{CH_3OH}}/2}}{1 - e^{-\beta\hbar\omega_{\mathrm{tor}}^{\mathrm{CH_3OH}}}}. \tag{9}$$

This may not be a good approximation at high temperatures, so we have calculated the torsional potential about the C–O bond by performing MC3BB calculations every 5°, in which all geometric parameters were optimized with the exception of the dihedral angle. The calculations were carried out on methanol and on both transition states, TS-R1 and TS-R2. The results are plotted in Fig. 2. It should be noticed that the two chiral transition states of reaction R1 are now connected by the torsional potential, so instead of using the HO partition function and include the symmetry number of Eq. (8), which accounts for the two enantiomers, it is better to consider a multiconformer harmonic-oscillator (MC-HO) partition function, which, in general, is given by[91]

$$Q_{\mathrm{tor}}^{\mathrm{MC-HO}} = \sum_{j=1}^{P} \frac{e^{-\beta(U_j + \hbar\omega_{\mathrm{tor,j}}/2)}}{1 - e^{-\beta\hbar\omega_{\mathrm{tor,j}}}}, \tag{10}$$

where U_j is the energy of well j relative to the lowest well of the torsional potential, $\omega_{\mathrm{tor},j}$ is the harmonic frequency of well j, and the sum runs over the P distinguishable conformers. If there is only one conformer then Eq. (10) reduces to Eq. (9). For transition state TS-R1, $P = 2$, whereas for both TS-R2 and methanol $P = 1$ (so in this case we use either the HO or the MC-OH expression).

The one-dimensional hindered-rotor partition function can be calculated conveniently by the torsional eigenvalue summation (TES) method,[91] and we simplify the calculations by assuming that: (i) the reduced moment of inertia, I, is independent of the reaction coordinate and (ii) the potentials can be accurately fitted to a cosine Fourier series of the type,

$$V(\phi) = b_0 + \sum_{n=1}^{n_{\max}} b_n \cos(n\phi), \tag{11}$$

where $b_0, b_n, n = 1, \ldots, n_{\max}$ are parameters.

We have calculated the reduced moments of inertia of methanol, TS-R1, and TS-R2 at the equilibrium configurations using the scheme developed by Pitzer,[92] which allows the calculation of a single asymmetric top attached to a rigid frame. The calculated reduced moments of inertia (in atomic units) for methanol, TS-R1, and TS-R2 have values of 3956.3, 4439.8, and 12191, respectively. For the relaxed scans starting at each of the three stationary points, the largest variation of the reduced moment of inertia along the torsion coordinate with respect to the equilibrium value was smaller than 3%, so approximation (i) is very good in this case.

As shown in Fig. 2, the cosine Fourier series potentials for methanol,

$$V(\phi)_{\mathrm{CH_3OH}}/\mathrm{cm}^{-1} = 180.401 + 182.1\cos(3\phi) + 1.8\cos(6\phi), \tag{12}$$

TS-R1,

$$V(\phi)_{\mathrm{TS-R1}}/\mathrm{cm}^{-1} = 632.053 - 317.0\cos(\phi) + 548.3\cos(2\phi) + 119.9\cos(3\phi) + 23.0\cos(4\phi), \tag{13}$$

and TS-R2,

$$V(\phi)_{\mathrm{TS-R2}}/\mathrm{cm}^{-1} = 251.859 + 260.4\cos(3\phi) + 11.5\cos(6\phi) + 1.1\cos(9\phi), \tag{14}$$

fit the MC3BB torsion potential accurately.

The TES partition function is simply obtained from eigenvalue summation of the torsional coordinate, i.e.,

$$Q_{\text{tor}}^{\text{TES}} = \frac{1}{\sigma_{\text{tor}}} \sum_{j=0}^{j_{\max}} e^{-\beta E_j}, \tag{15}$$

where E_j are the energies (eigenvalues) obtained from solving the Schrödinger equation (see Ref. 91 for details) and $j_{\max}$ is the total number of eigenvalues, which should be large enough so that the calculated partition function is converged (usually $j_{\max} = 200$ suffices); σ_{tor} is the symmetry number due to torsion (number of indistinguishable minima due to internal rotation), which is the unity for TS-R1 and 3 for both methanol and TS-R2. The lowest eigenvalue of the TES method gives the zero-point energy of the torsional potential, and, therefore, the frequency associated to it. The harmonic frequencies associated to the C–O bond torsion in methanol, TS-R1, and TS-R2 are 290, 359, and 190 cm^{-1}, respectively, whereas the anharmonic frequencies obtained by the TES method are 250, 342, and 186 cm^{-1}, respectively.

We denote as $Q_{\text{tor}}^{\text{MC-HO-Z}}$ the ZPE corrected MC-HO partition function with the TES calculated frequencies. The total anharmonicity on the torsional mode is the product of two effects: (1) that due to corrections in the ZPE, which is given by the quotient $Q_{\text{tor}}^{\text{MC-HO-Z}}/Q_{\text{tor}}^{\text{MC-HO}}$ and (2) that due to the deviations from the HO approximation, which is given by the quotient $Q_{\text{tor}}^{\text{TES}}/Q_{\text{tor}}^{\text{MC-HO-Z}}$. As shown in Table II, in general, the anharmonicity is more important for the equilibrum configuration of methanol, when compared with the transition states TS-R1 and TS-R2 because the former has the lowest torsional barrier of the three of them. At low temperatures the ZPE effect is quite important, and at T =300 K there is an important ZPE effect in methanol that makes the MC-HO-Z partition function 16% higher than the MC-HO partition function. As the temperature increases more levels are populated, and the leading effect is the level separation, which remains constant in the harmonic oscillator whereas it may decrease in the anharmonic treatment. As a consequence, the harmonic partition function increases faster than the TES partition function and at T =2500 K it is 41% higher for the equilibrium configuration of methanol. This effect is also important for TS-R2 and at T =2500 K the MC-HO partition function is 28% higher than the TES partition function. For TS-R1, which has the largest torsional barriers of the three configurations considered here, the TES partition function is less than 10% higher than the MC-HO partition function at 300 and 2500 K (the discrepancy is larger at some intermediate temperatures, i.e., about 20% at T = 1000 K), so in general the harmonic approximation is better than for TS-R2 and for methanol.

III.C. Theoretical thermal rate constants

The thermal rate constants obtained by TST, CVT, CVT/ZCT, and CVT/μOMT methods for the hydrogen abstraction are listed in Table III. Note that here we use the acronym TST, or the superscript ‡, to denote conventional transition state theory results without tunneling but with anharmonic treatment of the C–O bond torsion. In fact all the thermal rate constants listed in Table III were obtained by multiplying the thermal rate constants obtained using the harmonic approximation for all the degrees of freedom by the coefficient, $\alpha_{\text{tor}}^{\ddagger}$, which includes the anharmonic effects on the torsional modes, i.e., for the TST thermal rate constant,

$$k_{\text{tor,TES}}^{\text{TST}} = \alpha_{\text{tor}}^{\ddagger} k_{\text{tor,MC-HO}}^{\text{TST}}, \tag{16}$$

where $k_{\text{tor,TES}}^{\text{TST}}$ and $k_{\text{tor,MC-HO}}^{\text{TST}}$ are the calculated TST thermal rate constants using the TES and MC-HO partition functions for the torsion, respectively. The coefficient between them is given by the following quotient between partition functions:

$$\alpha_{\text{tor}}^{\ddagger} = \frac{Q_{\text{tor}}^{\text{TES},\ddagger} Q_{\text{tor}}^{\text{MC-HO,CH}_3\text{OH}}}{Q_{\text{tor}}^{\text{TES,CH}_3\text{OH}} Q_{\text{tor}}^{\text{MC-HO},\ddagger}}. \tag{17}$$

In Eq. (17) the symbol ‡ refers to TS-R1 or to TS-R2 depending whether we are discussing reaction R1 or reaction R2, and CH_3OH refers to methanol in its equilibrium configuration.

At T = 300 K, the coefficients $\alpha_{\text{tor}}^{\text{TS-R1}}$ and $\alpha_{\text{tor}}^{\text{TS-R2}}$ are 0.93 because in both cases the anharmonicity is mainly due to the ZPE effect in methanol. At high temperatures both methanol and TS-R2 show important deviations from the MC-HO partition functions. This is not the case for TS-R1, so the quotient between partition functions deviates more from the harmonic oscillator approximation for R1 than for R2. For instance, at T = 2500 K $\alpha_{\text{tor}}^{\text{TS-R1}}$ and $\alpha_{\text{tor}}^{\text{TS-R2}}$ are 1.56 and 1.11, respectively. Since R1 is the dominant channel for the hydrogen abstraction reaction, the anharmonic treatment of the torsional mode slightly lowers the total thermal rate constants at room temperature and moderately rises them at high temperatures, when compared to the harmonic oscillator values.

TABLE II. Multiconformer harmonic-oscillator and torsional eigenvalue summation partition functions of methanol, TS-R1 and TS-R2, respectively.

	CH_3OH			TS-R1			TS-R2		
T (K)	MC-HO	MC-HO-Z	TES	MC-HO	MC-HO-Z	TES	MC-HO	MC-HO-Z	TES
300.00	0.664	0.788	0.793	1.031	1.092	1.134	1.061	1.082	1.183
400.00	0.916	1.078	1.070	1.448	1.527	1.623	1.436	1.463	1.615
500.00	1.164	1.363	1.322	1.855	1.952	2.121	1.808	1.841	2.024
700.00	1.652	1.929	1.763	2.653	2.787	3.128	2.546	2.593	2.771
1000.00	2.378	2.770	2.318	3.834	4.023	4.607	3.649	3.716	3.739
1500.00	3.582	4.168	3.069	5.786	6.068	6.876	5.483	5.583	5.071
2000.00	4.782	5.563	3.689	7.732	8.106	8.887	7.315	7.448	6.179
2500.00	5.982	6.957	4.226	9.674	10.142	10.683	9.146	9.312	7.141

TABLE III. Thermal rate constants (in cm^3 $molecule^{-1}$ s^{-1}) obtained with TST, CVT and with CVT with the ZCT and μOMT approximations for tunneling for reactions R1 an R2. All rate constants include the anharmonicity parameter of Eq. (17).

	R1				R2			
T(K)	TST	CVT	CVT/ZCT	CVT/μOMT	TST	CVT	CVT/ZCT	CVT/μOMT
298	1.67(–17)[a]	1.53(–17)	4.71(–17)	1.93(–16)	2.47(–21)	1.64(-21)	1.72(–20)	5.16(–20)
300	1.84(–17)	1.68(–17)	5.11(–17)	2.05(–16)	2.89(–21)	1.92(-21)	1.95(–20)	5.74(–20)
400	7.17(–16)	6.73(–16)	1.23(–15)	2.79(–15)	1.04(–18)	7.83(-19)	2.48(–18)	4.50(–18)
500	7.09(–15)	6.74(–15)	9.88(–15)	1.68(–14)	3.82(–17)	3.08(-17)	6.20(–17)	8.99(–17)
600	3.51(–14)	3.36(–14)	4.37(–14)	6.36(–14)	4.44(–16)	3.74(-16)	6.00(–16)	7.74(–16)
700	1.16(–13)	1.12(–13)	1.35(–13)	1.79(–13)	2.66(–15)	2.31(-15)	3.25(–15)	3.92(–15)
1000	1.20(–12)	1.16(–12)	1.27(–12)	1.46(–12)	7.76(–14)	7.06(-14)	8.32(–14)	9.10(–14)
1500	9.80(–12)	9.50(–12)	9.90(–12)	1.05(–11)	1.37(–12)	1.28(-12)	1.38(–12)	1.43(–12)
2000	3.32(–11)	3.21(–11)	3.29(–11)	3.41(–11)	6.76(–12)	6.41(-12)	6.67(–12)	6.82(-12)
2500	7.59(–11)	7.31(–11)	7.43(–11)	7.59(–11)	1.93(–11)	1.84(–11)	1.89(–11)	1.92(–11)

[a]Powers of ten in parenthesis.

The ZCT and μOMT transmission coefficients are given in Table IV. The LCT transmission coefficients are not listed because they were always smaller than the SCT ones; the latter coincided at all temperatures in the interval of temperatures 300–2500 K with the μOMT transmission coefficients. The barrier height for reaction R1 is much lower than that for reaction R2, and the dynamics calculations confirm that reaction R1 is faster than reaction R2 between 300 and 2500 K and only at high temperatures does the contribution of R2 start to be important. Tunneling is more important for reaction R2, with the μOMT transmission coefficient at $T = 300$ K being 29.8 (2.45 times larger than for reaction R1.) However, the variational effects decrease the rate constants at $T = 300$ K by a factor of 0.67, and the CVT/μOMT rate constant is just 19.9 times larger than the TST one. For reaction R1, tunneling is less important, but variational effects are very small, and, therefore, at $T = 300$ K the CVT/μOMT rate constant is 11.2 times larger than the TST result, with a μOMT transmission coefficient of 12.2. It is important to include the coupling between the reaction coordinate and the normal modes orthogonal to it because the ZCT transmission coefficients seriously underestimate the tunneling contribution for both reactions. It should be noticed that the ZCT transmission coefficient is multidimensional because it includes the variation of $\epsilon^G_{\rm int}(s)$ with s, which is a multidimensional effect, but it treats the MEP as if it were one dimensional by neglecting its curvature, although it is a multidimensional path.

TABLE IV. Transmission coefficients computed with the ZCT and μOMT approximations for R1 and R2 reactions.

	R1		R2	
T (K)	CVT/ZCT	CVT/μOMT	CVT/ZCT	CVT/μOMT
300	3.03	12.2	10.1	29.8
400	1.83	4.14	3.17	5.74
500	1.47	2.50	2.01	2.92
700	1.21	1.60	1.41	1.69
1000	1.10	1.26	1.18	1.29
1500	1.04	1.11	1.07	1.12
2000	1.02	1.06	1.04	1.06
2500	1.02	1.04	1.03	1.04

The Wigner[34] and Eckart[35] tunneling contributions used by Lendvay *et al.*[19] and by Jodkowski *et al.*,[26] respectively, are obtained from the second derivative of $V_{\rm MEP}(s)$ at the top of the potential, i.e., those are completely one-dimensional models based on the normal mode with imaginary frequency at the transition state. The imaginary frequencies at the MC3BB level for reactions R1 and R2 are, respectively, $1466i$ and $1718i$ cm^{-1}, and with values of the Wigner transmission coefficients at $T = 300$ K of 3.06 and 3.83. (The failure of the Wigner model is not surprising when one considers that the value of 3.83 results from retaining only the first two terms of a series that begins $1 + 2.83 + \cdots$.) The transmission coefficients predicted by the Wigner expression are too small. However, the transmission coefficients reported by Jodkowski *et al.*,[26] which were based on the Eckart potential are unusually large with values of 7.5 and 27.2 at $T = 400$ K for reactions R1 and R2, respectively, as compared to the μOMT transmission coefficients of 4.1 and 5.7. Those authors obtained such a large values because their calculations used imaginary frequencies with values of $1827i$ and $2246i$ cm^{-1} for reactions R1 and R2, respectively. In one-dimensional models, larger imaginary frequencies always lead to narrower potentials and, therefore, to larger transmission coefficients (see Fig. 3). In multidimensional models, such as μOMT, this is not so straightforward because although very close to the transition state the reactive motion can be regarded as one dimensional (at that stage the reaction coordinate involves essentially the motion of the atoms of the mode with imaginary frequency), as the reaction progresses toward reactants and toward products more normal mode motions get involved and coupling between the reaction coordinate and the other modes becomes important. As a consequence, the magnitude of the tunneling effect does not depend exclusively on the magnitude of the imaginary frequency at the transition state, although is still a useful but rough indication of the amount of tunneling.

Kerkeni and Clary[28] reported values for the imaginary frequencies calculated at the MP2(full)/cc-pVTZ level which are $1802i$ and $2158i$ cm^{-1} for reactions R1 and R2,

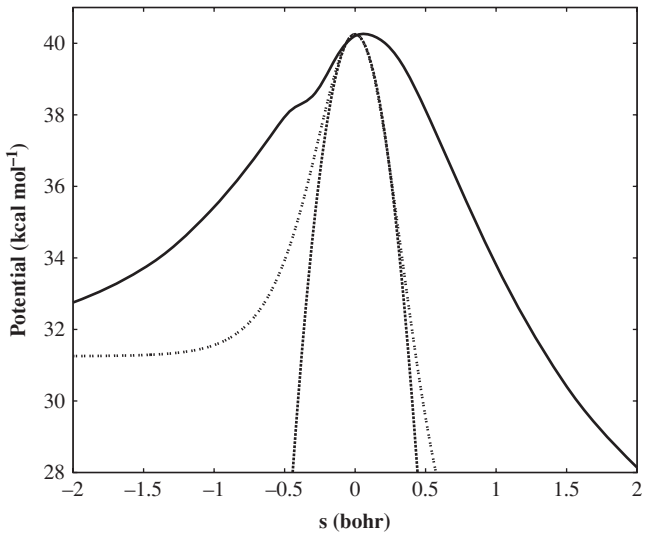

FIG. 3. Vibrationally adiabatic potential for reaction R1 (solid line) compared to Wigner (inverse parabola) and Eckart potentials that were obtained with the imaginary frequency reported in Ref. 26 for reaction R1, i.e., $1827i$ cm^{-1}. The three potentials are normalized to the same value at the saddle point ($s = 0$).

respectively. These large values are obtained because the MP2(full)/cc-pVTZ level yields barrier heights which are too high in this case (i.e., 14.4 and 24.4 kcal/mol for reactions R1 and R2, respectively), making the potential near to the top of the barrier too narrow. For this reason their tunneling calculations are 42% larger than our μOMT transmission coefficients at $T = 300$ K. (For reactions R1 and R2, the μOMT transmission coefficients are about 12 and 30, whereas those obtained by Kerkeni and Clary[28] are about 17 and 38.) At $T = 700$ K, the agreement is very good for reaction R1 but less satisfactory for reaction R2, with the transmission coefficients reported by them being about 1.7 and 4.3, for reactions R1 and R2, respectively. As we have mentioned previously, at high temperatures most of the tunneling (if any) occurs near the top of the barrier and the magnitude of the transmission

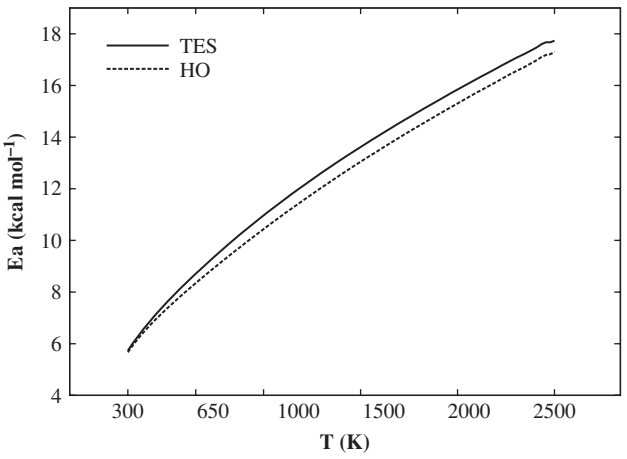

FIG. 4. Variation of the activation energy (in kcal/mol) with temperature for the total CH_3OH + H reaction (R1 + R2). HO and TES refer, respectively, to the harmonic oscillator and the torsional eigenvalue summation treatments given to the torsional mode.

coefficient is more sensitive to the value of the imaginary frequency, which in this case is too high.

The issues raised in this discussion point out the importance of choosing electronic structure methods consistent not just with the energetics of the reaction (which can often be achieved by performing very accurate single-point calculations on optimized geometries obtained at a lower level), but also with other aspects of the potential energy surface, such as geometries and vibrational frequencies, which may have an important impact on the dynamics. On the other hand, the multidimensional methods for tunneling show the limited reliability of one-dimensional methods, since the latter do not account for many of the features of the chemical reaction.

III.D. Arrhenius parameters

Table V lists the Arrhenius parameters obtained by different experimental techniques or by different theoretical methods for the R1 + R2 hydrogen abstraction process. The discharge flow reactor experiments are available at temperatures ranging from 295 to 680 K, which is a temperature region in which quantum effects are very relevant. To establish some difference between these data and those obtained from high-temperature experiments (as for instance pyrolysis and unimolecular decomposition), all data were divided into two sets, one "low-temperature" (low T) set for data between 295 and 700 K and one "high-temperature" (high T) set for data which are roughly between 700 and 2000 K. Although we do not recommend two-parameter Arrhenius fits in general, we made such fits in Table V simply as a convenient way to make comparisons.

Whereas the activation energies in Table V represent averages over given temperature intervals, it is also interesting to consider the temperature-dependent activation energy given by the local slope of an Arrhenius plot as

$$E_a = -R\frac{d\ln k}{d(\frac{1}{T})}. \tag{18}$$

Figure 4 plots E_a as a function of temperature and shows that the anharmonicity in the torsional mode increases the energy of activation regarding to the harmonic treatment. Besides, E_a increases substantially with temperature, i.e., from 5.73 kcal/mol (5.67 kcal/mol with the harmonic approximation) at $T = 300$ K to 17.7 kcal/mol (17.3 kcal/mol using the harmonic approximation) at $T = 2500$ K. This behavior is not just due to the quantum effects, which decrease both the pre-exponential factor and the activation energy at low T with respect to the classical rate constant because the TST activation energy also increases when going from low T to high T in values averaged over intervals (see Table V); using Eq. (18) with TST gives 8.6 kcal/mol at $T = 300$ K and 18.3 kcal/mol at $T = 2500$ K. The change of the activation energy with temperature is typical of many bimolecular gas-phase reaction rate constants,[93–96] and it leads to curved Arrhenius plots. Figure 5 shows a concave Arrhenius plot even at high T which is an indication of the rise of the activation energy with temperature.

On the basis of the rigorous definition given by Tolman[97,98] in which the activation energy is interpreted as

TABLE V. Arrhenius parameters (activation energies E_a, in kcal/mol, and logarithm (to the base 10) of the pre-exponential factor, $\log(A/\text{cm}^3\,\text{s}^{-1}\,\text{molecule}^{-1})$ for the overall $CH_3OH + H$ reaction.

Reference	T(K)	log$A$	E_a	Experimental technique/Theoretical method
Aders and Wagner[20]	295–653	– 10.42	5.30	Discharge flow reactor
Meagher *et al.*[21]	298–575	– 10.96	5.44	ESR
Warnatz[3]	300–700	– 10.18	6.10	Combustion
Hoyermann *et al.*[18]	500–680	– 10.66	5.29	Discharge flow reactor
Li and Williams[10]	300–700	– 9.95	6.75	Laminar counterflow flame
Baulch *et al.*[23]	300–700	– 10.40	5.60	Fit to values of Refs. 14, 16, 18, and 20
Chuang *et al.*[27]	300–700	– 10.93	4.11	CVT/μOMT
Lendvay *et al.*[19]	300–700	– 9.53	6.96	TST/Wigner
Jodkowski *et al.*[26]	300–700	– 11.00	6.13	TST/Eckart
Carvalho *et al.*[32]	300–600	– 10.66	6.59	IVTST-0/ZCT
Kerkeni and Clary[28]	320–680	– 10.76	6.59	Reduced dimensionality QD
This work	300–700	– 10.11	9.17	TST
This work	300–700	– 10.59	7.18	CVT/μOMT
Westbrook and Dryer[1]	1000–2180	– 10.28	7.01	Pyrolysis
Vandooren and Tiggelen[14]	1000–2000	– 10.25	2.61	Beam molecular sampling
Spindler and Wagner[15]	1600–2100	– 10.28	5.25	Thermal unimolecular decomposition
Warnatz[3]	700–2000	– 10.18	6.10	Combustion
Cribb *et al.*[16]	1800–2740	– 9.32	14.06	Pyrolysis
Li and Williams[10]	700–2000	– 9.02	9.90	Laminar counterflow flame
Held and Dryer[7]	633–2050	– 10.52	6.10	Several experimental techniques
Tsang[22]	600–2000	– 9.08	9.37	Fit to BEBO calculations
Baulch *et al.*[23]	700–2000	– 9.88	7.36	Fit to values of Refs. 14, 16, 18, and 20
Chuang *et al.*[27]	700–2000	– 9.75	7.34	CVT/μOMT
Lendvay *et al.*[19]	700–2000	– 8.82	9.37	TST/Wigner
Jodkowski *et al.*[26]	700–2000	– 9.38	11.19	TST/Eckart
Carvalho *et al.*[32]	800–2000	– 9.31	11.18	IVTST-0/ZCT
Kerkeni and Clary[28]	680–2000	– 9.97	9.11	Reduced dimensionality QD
This work	700–2000	– 9.09	12.67	TST
This work	700–2000	– 9.18	11.84	CVT/μOMT

the average energy over all reacting molecules minus the average energy over all reactant molecules (independently of whether they react or not), it is possible to interpret the change of the activation energy with temperature.[94,99,100] Basically, an activation energy that increases with temperature means that at higher temperatures the average energy of reacting systems is increasing more rapidly than the average energy of all possible reactants. From the point of view of TST, the variation of the activation energy with temperature depends strongly on the magnitude of the transitional modes (the normal modes at the transition state structure coming from the rotational and translational motions of reactants),[101] an issue that was already pointed out by Meagher *et al.*[21] for the overall $CH_3OH + H$ reaction.

From the experimental point of view only the measurements of Li and Williams[10] are available at low T and high T and in this case a clear increase of the activation energy with temperature is observed. With the exception of this work and that of Cribb *et al.*[16] the high T experiments do not show a clear increase of the activation energy with respect to the low T experiments, so we believe that those high T experiments deserve further checking. It should be also noticed that most of the experimental data reported (listed in Table V) were fitted to Arrhenius expressions (the work of Li and Williams[10] is an exception). Some of these Arrhenius parameters were later on used in the modeling of the mechanism of combustion and oxidation of methanol;[8,11] the approximation of uncurved Arrhenius plots could affect the conclusions of those studies.

Figure 5 shows that our CVT/μOMT results are very similar to the reduced dimensionality quantum dynamics results of Kerkeni and Clary[28] till about $T = 1000$ K, and at higher temperatures they are closer to the thermal rate constants calculated by Jodkowski *et al.*[26] In the interval of temperatures at which the discharge flow reactor experiments by Aders and Wagner[20] were carried out and the ESR experiments by Meagher *et al.*[21] were performed, the calculated CVT/μOMT thermal rate constants lay below those values because the theoretical calculations lead to a much higher activation energy. The experimental data of Hoyermann *et al.*[18] are about six and three times larger than the CVT/μOMT results at $T = 500$ and 680 K, respectively, indicating also that their results have a more nearly constant slope. Actually, their results have the same slope as the values reported by Aders and Wagner,[20] which is surprising because the measurements by Hoyermann *et al.*[18] start at temperatures about 200 K higher; therefore, a larger activation energy would be expected. Meagher *et al.*[21] pointed out that, since their ESR experiments measure the disappearance of the H atom radical (the discharge flow reactor experiments also measure that concentration) part of the hydrogen radical could be consumed by the side reaction $CH_2OH + H \rightarrow CH_3 + OH$.

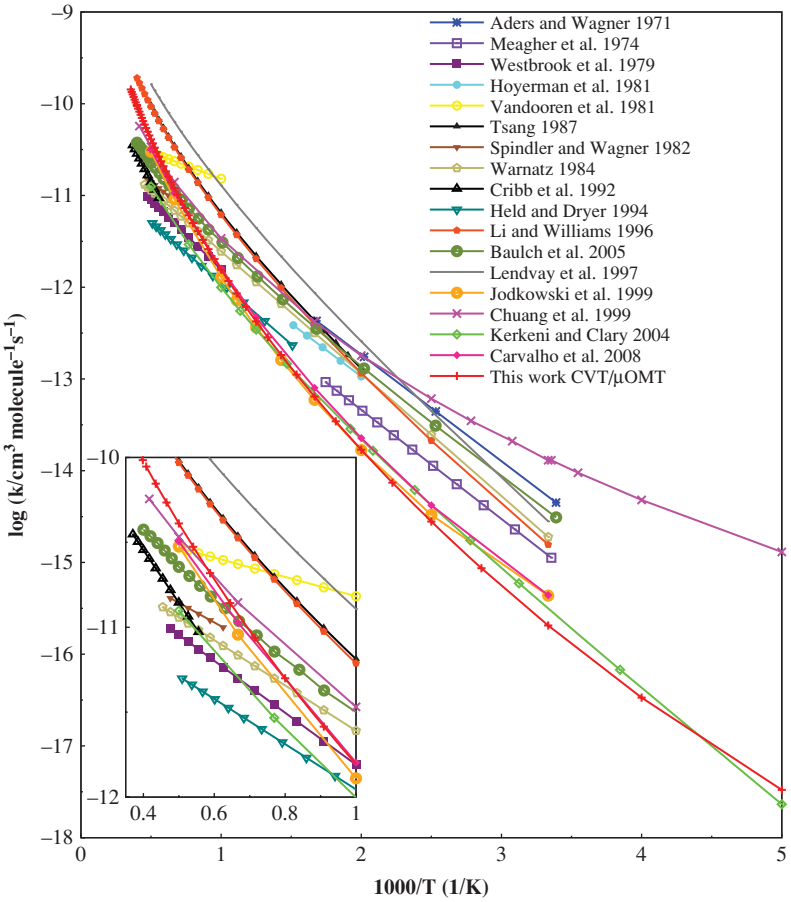

FIG. 5. Arrhenius plot that compares the CVTμOMT total (R1 + R2) thermal rate constants computed at the MC3BB level with experimental and theoretical works available in the literature. The left-bottom corner of the figure is a zoom with the data at high temperatures.

However, both, the pre-exponential factor obtained, which is typical of that for a hydrogen abstraction reaction, and the high linearity in the decay of the hydrogen radical concentration, suggest that side reaction is unimportant. This is still a controversial issue because some of the modeling involved in the study of the mechanism of combustion of methanol[5,7,8] indicate its importance in the consumption of hydrogen radical and in the generation of OH radicals.

At high T reliable values of the thermal rate constants for reactions R1 and R2 are very important because most of the modeling of the combustion of methanol is carried out at these temperatures. The diversity of the values of the rate constants (see Table V and left corner of Fig. 5) indicates a great uncertainty in the experimental data. Because the energy of activation changes with temperature, the data are only comparable at the same interval of temperatures; nevertheless most of the data are incongruent with the low T experiments. Thus, the experiments of Westbrook and Dryer,[1] Warnatz,[3] Vandooren and Tiggelen,[14] Spindler and Wagner,[15] and Held and Dryer[7] lead to activation energies which are too low as compared to theory. Cribb *et al.*[16] reported a value for the activation energy of 14.1 kcal/mol for the interval between $T = 1800$ and 2740 K that is in relatively good agreement with the value of 16.7 kcal/mol obtained by CVT/μOMT for the same interval.

As mentioned above the large dependence of the activation energy on temperature discourages the use of Arrhenius expression for the overall R1 + R2 reaction even in small temperature ranges. One alternative to the equation of Arrhenius which is widely used in practice is

$$k(T) = A\left(\frac{T}{300}\right)^n e^{-E/T}, \tag{19}$$

where A, n, and E are parameters and T is temperature. As shown in Refs. 100 and 101, Eq. (19) fits perfectly the curved Arrhenius plot only if the activation energy increases linearly with temperature, which is not the case here. However, at temperatures of combustion, as shown in Fig. 4, the dependence of E_a with temperature is almost linear, so in Table VI we report values of the A, n, and E fitting parameters for the total thermal rate constants above $T = 700$ K. To reproduce well the whole interval between $T = 300$ and 2500 K, it is necessary to use a more elaborate expression that reproduces the asymptotic behavior at low temperatures, i.e.,[102]

$$k(T) = A\left(\frac{T}{300}\right)^n \exp\left[\frac{-E(T+T_0)}{T^2+T_0^2}\right]. \tag{20}$$

This equation has four fitting parameters A, n, E, and T_0. The errors are calculated as the value of the root mean square residual (RMSR), which is given by

$$\mathrm{RMSR} = \left\{\frac{1}{N}\left[\sum_{i=1}^{N} \ln\left(\frac{k(T_i)}{k_M(p_1, \ldots, p_K, T_i)}\right)\right]^2\right\}^{1/2}, \tag{21}$$

TABLE VI. Fitting parameters to the CVT/μOMT thermal rate constants for the total reaction R1 + R2 and for R1 and R2 using Eqs. (19) and (20). The RMSR values are also given.

	Reaction		
Parameter	R1 + R2	R1	R2
Eq. (19) ($700 \leq T \leq 2500$)			
A (cm^3 s^{-1} molecule^{-1})	1.170×10^{-12}	1.713×10^{-12}	1.898×10^{-12}
n	2.612	2.351	2.147
E (K)	2850	2975	5603
RMSR	0.017	0.014	0.010
Eq. (20) ($300 \leq T \leq 2500$)			
A (cm^3 s^{-1} molecule^{-1})	4.738×10^{-13}	7.334×10^{-13}	3.504×10^{-13}
n	2.922	2.632	2.707
E (K)	2005	2128	4008
T_0 (K)	204.5	208.7	188.8
RMSR	0.017	0.016	0.011

where N is the number of temperatures, which in this case were taken every 10 K; $k(T_i)$ is the CVT/μOMT thermal rate constant at T_i, and $k_M(p_1, ..., p_K, T_i)$ are the fitted thermal rate constants involving the K parameters given by Eq. (19) ($K = 3$) or by Eq. (20) ($K = 4$). All parameters are listed in Table VI. Since Eq. (19) is only used at high temperatures, the RMSR values are very small for both fits. We recommend Eq. (20) at low and midrange T, and either fit may be used at temperatures above $T = 700$ K.

III.E. Branching ratios

Reactions R1 and R2 obtained by CVT/μOMT were also fitted to Eqs. (19) and (20). The results are given in Table VI. With the exception of the experiments of Li *et al.*,[11] all the theoretical and experimental data plotted in Fig. 6 show that reaction R1 dominates over the whole range of temperatures 300–2500 K. All the theoretical works show some temperature dependence of the branching ratio with temperature. The CVT/μOMT calculations with the torsional mode treated within the harmonic approximation and the work of Lendvay *et al.*[19] predict similar branching ratios, with percentages that never reach 30% even at $T = 2000$ K, whereas the works of Kerkeni and Clary[28] and Jodkowski *et al.*[26] predict even smaller percentages for reaction R2. When anharmonicity is included the branching ratio increases, and at $T = 2000$ K, R1 contributes about 80% to the total abstraction reaction. In this context, the assumption of Held and Dryer[7] seems quite unrealistic because they consider that the branching ratio is independent of temperature, which is equivalent to assuming that both reactions have the same activation energy. On the other hand, the results reported by Li *et al.*[11] indicate that at $T = 500$ K, R2 contributes by more than 30% to the total abstraction reaction, and at about $T = 800$ K reaction R2 starts to dominate. However, at temperatures between 500 and 680 K, Hoyermann *et al.*[18] by doing deuterium isotopic substitution of methanol with the further analysis of the products showed, although not conclusively, that reaction R1 is the main channel for hydrogen abstraction from methanol. The theoretical calculations also support that conclusion. The comparison of theory and experiment for the branching ratio between reactions R1 and R2 brings into question the accuracy of the experimental results, so we recommend the use of Eqs. (19) and (20) with the parameters of Table VI for the study of mechanisms related to the combustion of methanol.

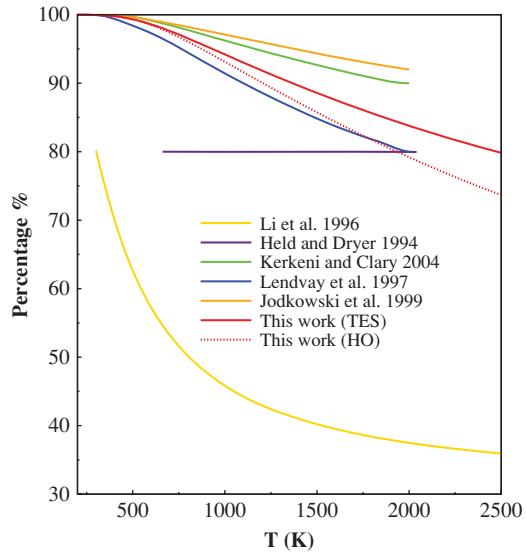

FIG. 6. Branching ratio expressed as a percentage: $(k_{R1}/(k_{R1} + k_{R2})) \times 100$. Several theoretical and experimental data are plotted. HO and TES have the same meaning as in Fig. 4.

III.F. Kinetic isotope effects

The KIE is an important tool to study reaction mechanisms and analyze tunneling effects. We have calculated two KIEs at low temperatures (at which only R1 contributes significantly to the total abstraction rate constant), i.e., the secondary KIE defined as the reaction rate ratio between reactions R1 and R4, $\eta_{1,4}(T)$, and the primary KIE given by the ratio between reactions R1 and R5, $\eta_{1,5}(T)$. We use the notation

$$\eta(T) = \frac{k_H(T)}{k_D(T)}, \tag{22}$$

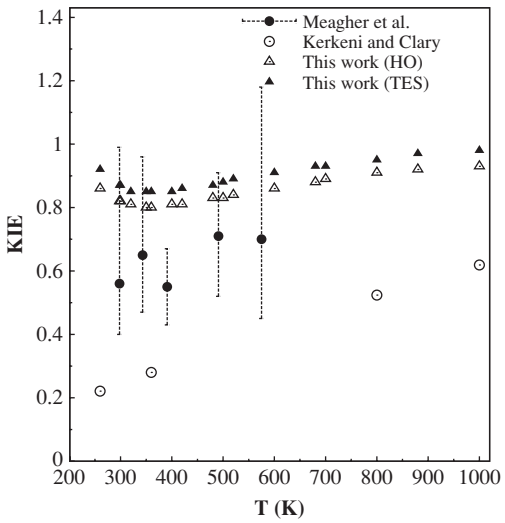

FIG. 7. Values of $\eta_{1,4}$ between $T = 250$ and 1000 K. The experimental data of Ref. 21 are indicated with error bars. HO and TES have the same meaning as in Fig. 4.

where $k_H(T)$ is the rate constant for reaction R1 and $k_D(T)$ is that for R4 or R5 reactions.

The KIEs are factorized into their quasiclassical, $\eta_{QC}(T)$, and tunneling, $\eta_{tun}(T)$ contributions, i.e.,

$$\eta(T) = \eta_{tun}(T)\eta_{QC}(T), \tag{23}$$

where

$$\eta_{tun}(T) = \frac{\kappa_H^{CVT/\mu OMT}(T)}{\kappa_D^{CVT/\mu OMT}(T)}, \tag{24}$$

and $\eta_{QC}(T)$ is given by

$$\eta_{QC}(T) = \eta_{var}(T)\eta^{TST}(T), \tag{25}$$

where $\eta_{var}(T)$ is the variational contribution to the KIE and $\eta^{TST}(T)$ is the TST contribution to the KIE and is given by

$$\eta^{TST}(T) = \eta_{trans}\eta_{rot}^{TST}\eta_{vib,tor}^{TST}(T), \tag{26}$$

where η_{trans} and η_{rot}^{TST} are the translational and rotational temperature-independent contributions and $\eta_{vib,tor}^{TST}(T)$ is the temperature-dependent vibrational contribution in which the torsional mode was treated using the TES method.

The experimental data of Meagher *et al.*[21] (see Fig. 7) show that the secondary KIE $\eta_{1,4}$ is inverse (smaller than the unity). Both sets of theoretical results shown in Fig. 7 also exhibit this tendency, although our CVT/μOMT results are in better agreement with the experimental data. The contributions to the KIE are listed in Table VII. The product of translational and rotational contributions does not change with temperature and equals 2.00. The anharmonic contribution of the torsional mode to the KIE is quite modest and the largest difference with respect to the harmonic oscillator treatment occurs at low T and is about 7%. The vibrational and variational contributions are smaller than unity, and at $T = 300$ K their product is 0.26, which gives a quasiclasical KIE of 0.43. The experimental KIEs have significant error bars and are roughly between 0.4 and 1.2, with the data clustered between 0.5 and 0.7. The CVT/μOMT results show

TABLE VII. Contributions to the KIE $\eta_{1,4}$ (see text) obtained at the MC3BB level and using the CVT/μOMT thermal rate constants.[a] Both $\eta_{vib,HO}^{TST}$ and $\eta_{vib,tor}^{TST}$ are the vibrational contributions to the KIE using, respectively, the harmonic oscillator and TES approximations to the torsional mode.

T (K)	$\eta_{vib,HO}^{TST}$	$\eta_{vib,tor}^{TST}$	η^{TST}	η_{var}	η_{QC}	η_{tun}	$\eta_{1,4}$
300	0.24	0.26	0.47[a]	0.91	0.43	1.84	0.87
400	0.32	0.33	0.62	0.93	0.58	1.36	0.85
500	0.37	0.38	0.72	0.95	0.69	1.20	0.88
700	0.42	0.44	0.83	0.96	0.82	1.09	0.93
1000	0.46	0.48	0.90	0.96	0.91	1.04	0.98
1500	0.49	0.51	0.95	0.96	0.95	1.02	1.01

[a] $\eta_{trans} = 2.70$; $\eta_{rot}^{TST} = 0.74$.

that tunneling increases the total KIE because a multidimensional effect that greatly favors tunneling in reaction R1 over reaction R4 is that the vibrationally adiabatic barrier height is larger for the former reaction, i.e., 8.48 kcal/mol, whereas for reaction R4 is 7.72 kcal/mol. At $T = 300$ K this leads to μOMT transmission coefficients which are 12.2 and 6.63 for reactions R1 and R4, respectively, increasing the KIE by a factor of 1.84 and leading to a final predicted value for the KIE in good agreement with experiment.

The contributions to the calculated CVT/μOMT primary KIE $\eta_{1,5}$ are listed in Table VIII. The final predicted KIE agrees quite well with the experimental data obtained by Hoyermann *et al.*[18] (see Fig. 8), although the KIEs obtained from their raw data may be unreliable because the thermal rate constants reported by them have large error bars. They also fitted the thermal rate constants for R5 and for R6 to the same Arrhenius expression. This looks like a good approximation since our CVT/μOMT calculations for R6 deviate less than 2% from those obtained for R5 in the temperature range 300–2500 K, so we do not report those values here. The translational, rotational, and variational contributions are very close to unity, and their product leads to a value of only 1.29 at $T = 300$ K, so the main contribution to the quasiclassical KIE is due to vibration. For the factorization employed in Table VIII, the vibrational contribution to the KIE is given by

$$\eta_{vib,tor}^{TST} = \frac{Q_{vib,tor}^{TS-R1} Q_{vib,tor}^{CD_3OH}}{Q_{vib,tor}^{TS-R5} Q_{vib,tor}^{CH_3OH}}, \tag{27}$$

where $Q_{vib,tor}^{TS-R1}$ and $Q_{vib,tor}^{TS-R5}$ are the vibrational partition functions of the conventional transition states (saddle points)

TABLE VIII. Same as Table VII but for $\eta_{1,5}$.

T (K)	$\eta_{vib,HO}^{TST}$	$\eta_{vib,tor}^{TST}$	η^{TST}	η_{var}	η_{QC}	η_{tun}	$\eta_{1,5}$
300	6.50	7.30	8.65[a]	0.78	7.29	2.24	20.99
400	3.95	4.45	5.27	0.83	4.64	1.70	9.45
500	2.92	3.29	3.89	0.87	3.52	1.44	5.83
700	2.08	2.33	2.77	0.90	2.56	1.22	3.46
1000	1.63	1.84	2.18	0.92	2.04	1.11	2.45
1500	1.40	1.57	1.86	0.93	1.75	1.05	1.97

[a] $\eta_{trans} = 1.01$; $\eta_{rot}^{TST} = 1.18$.

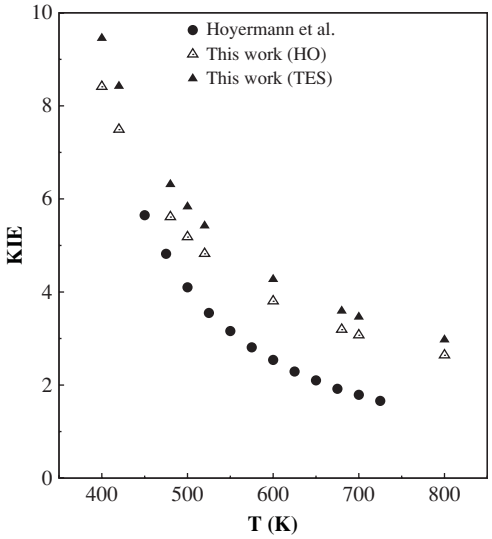

FIG. 8. Values of $\eta_{1,5}$ between $T = 250$ and 1000 K. HO and TES have the same meaning as in Fig. 4.

of the R1 and R5 reactions, respectively, and $Q_{\text{vib,tor}}^{\text{CD}_3\text{OH}}$ and $Q_{\text{vib,tor}}^{\text{CH}_3\text{OH}}$ are the reactant vibrational partition functions of CD_3OH and CH_3OH, respectively. All of them include the calculation of the torsional mode partition function by the TES method. The vibrational KIE is larger than the unity because the quotient between reactants partition functions is quite big mainly due to the difference in the value of the frequencies of the C–D and C–H stretches. This mass effect largely compensates the quotient between the vibrational partition function of the transition states, which is smaller than the unity. In the case of the $\eta_{1,4}$ KIE, the latter is the only contribution to the vibrational KIE, because the vibrational frequencies of reactants are the same. Moreover, the anharmonic treatment of the torsional mode increases the vibrational contribution to the KIE by about 10%.

In this case, it is also easy to understand that the tunneling contribution increases the KIE, since the hydrogen atom is lighter than deuterium, and, therefore, it has a larger probability of penetrating the barrier, if the barriers are the same. In the SCT and μOMT approximations, the effective barriers are not the same, but still the expected trend holds.

This last section shows that, although most of the theoretical models discussed in this paper predict similar thermal rate constants for the hydrogen abstraction reactions, a multidimensional tunneling method is needed in order to obtain good agreement with some of the KIEs.

IV. CONCLUSIONS

In the present work, we have performed high-level MC3BB direct-dynamics CVT/μOMT calculations in the temperatures interval 300–2500 K for the two competing hydrogen abstraction reactions R1 and R2 from methanol by atomic hydrogen. We have pointed out the importance of using multidimensional models for treating tunneling, which, with other factors being equal, provide both more reliable absolute thermal rate constants and kinetic isotope effects. It turned out that at high temperatures the anharmonicity of the torsional mode about the C–O bond plays an important role because it leads to thermal rate constants that deviate substantially from those obtained by the harmonic oscillator approximation. On the other hand, our calculations and previous theoretical works clearly indicate that the activation energy for the overall R1 + R2 process increases substantially with temperature; a conclusion not supported by the high T experimental data (above $T = 700$ K), which do not show a clear trend. For this reason for reactions R1 + R2, R1 and R2 we recommend the use of Eq. (20) in the whole range of temperatures, although Eq. (19) can also be used at high T. We propose these equations (in detriment of the Arrhenius equation) for further studies involving these reactions (as, for instance, combustion reactions). Reaction R1 dominates at all temperatures in the interval 300–2500 K, contributing 100% at room temperature and about 75% at $T = 2500$ K, so the branching ratio R1/R2 changes with temperature. Our calculated KIEs are in quite good agreement with experiment.

ACKNOWLEDGMENTS

A. F.-R. and R. M.-P. thank Xunta de Galicia for financial support through "Axuda para a Consolidación e Estructuración de unidades de investigación competitivas do Sistema Universitario de Galicia, 2007/50, cofinanciada polo FEDER 2007–2013." This work was supported in part by the U.S. Department of Energy (DOE), office of Basic Energy Sciences, through Grant No. DE-FG02-86ER13579 (2009) and as part of the Combustion Energy Frontier Research Center (2010).

[1] C. K. Westbrook and F. L. Dryer, Combust. Sci. Technol. **20**, 125 (1979).
[2] J. Dove and J. Warnatz, Ber. Bunsenges. Phys. Chem. **87**, 1040 (1983).
[3] J. Warnatz, *Combustion Chemistry* (Springer-Verlag, New York, 1984), p. 197.
[4] T. S. Norton and F. L. Dryer, Int. J. Chem. Kinet. **22**, 219 (1990).
[5] H.-H. Grotheer, S. Kelm, H. S. T. Driver, R. J. Hutcheon, R. D. Lockett, and G. N. Robertson, Ber. Bunsenges. Phys. Chem. **96**, 1360 (1992).
[6] B. Yang and K. Seshadri, Combust. Sci. Technol. **97**, 193 (1994).
[7] T. J. Held and F. L. Dryer, Sym. (Int.) Combust., [Proc.] **25**, 901 (1994).
[8] T. J. Held and F. L. Dryer, Int. J. Chem. Kinet. **30**, 805 (1998).
[9] K. Seshadri, Symp. (Int.) Combust., [Proc.] **26**, 831 (1996).
[10] S. C. Li and F. A. Williams, Symp. (Int.) Combust., [Proc.] **26**, 1017 (1996).
[11] J. Li, Z. Zhao, A. Kazakov, M. Chaos, F. Dryer, and J. J. Scire, Jr., Int. J. Chem. Kinet. **39**, 109 (2007).
[12] P. S. Veloo, Y. L. Wang, F. N. Egolfopoulos, and C. K. Westbrook, Combust. Flame **157**, 1989 (2010).
[13] R. T. Skodje, A. S. Tomlin, S. J. Klippenstein, L. B. Harding, and M. J. Davis, J. Phys. Chem. A **114**, 8286 (2010).
[14] J. Vandooren and P. J. V. Tiggelen, Symp. (Int.) Combust., [Proc.] **18**, 473 (1981).
[15] K. Spindler and H. G. Wagner, Ber. Bunsenges. Phys. Chem. **86**, 2 (1982).
[16] P. H. Cribb, J. E. Dove, and S. Yamazaki, Combust. Flame **88**, 169 (1992).
[17] D. Aronowitz, D. W. Naegeli, and I. Glassman, J. Phys. Chem. **81**, 2555 (1977).
[18] K. Hoyermann, R. Sievert, and H. G. Wagner, Ber. Bunsenges. Phys. Chem. **85**, 149 (1981).
[19] G. Lendvay, T. Bérces, and F. Márta, J. Phys. Chem. A **101**, 1588 (1997).
[20] W. K. Aders and H. G. Wagner, Z. Phys. Chem. **74**, 224 (1971).
[21] J. F. Meagher, P. Kim, J. H. Lee, and R. B. Timmons, J. Phys. Chem. **78**, 2650 (1974).
[22] W. Tsang, J. Phys. Chem. Ref. Data **16**, 471 (1987).

[23] D. L. Baulch, C. T. Bowman, C. J. Cobos, R. A. Cox, T. Just, J. A. Kerr, M. J. Pilling, D. Stocker, J. Troe, W. Tsang, R. W. Walker, and J. Warnatz, J. Phys. Chem. Ref. Data **34**, 757 (2005).
[24] P. Blowers, L. Ford, and R. Masel, J. Phys. Chem. A **102**, 9267 (1998).
[25] T. Zhu, J. Li, D. A. Liotard, C. J. Cramer, and D. G. Truhlar, J. Chem. Phys. **110**, 5503 (1999).
[26] J. T. Jodkowski, M. T. Rayez, J. C. Rayez, T. Bérces, and S. Dobé, J. Phys. Chem. A **103**, 3750 (1999).
[27] Y.-Y. Chuang, M. L. Radhakrishnan, P. L. Fast, C. J. Cramer, and D. G. Truhlar, J. Phys. Chem. A **103**, 4893 (1999).
[28] B. Kerkeni and D. C. Clary, J. Chem. Phys. **121**, 6809 (2004).
[29] B. Kerkeni and D. C. Clary, J. Phys. Chem. A **108**, 8966 (2004).
[30] J. Pu and D. G. Truhlar, J. Phys. Chem. A **109**, 773 (2005).
[31] E. F. V. Carvalho, A. N. Barauna, F. B. C. Machado, and O. Roberto-Neto, Int. J. Quantum Chem. **108**, 2476 (2008).
[32] E. F. V. Carvalho, A. N. Barauna, F. B. C. Machado, and O. Roberto-Neto, Chem. Phys. Lett. **463**, 33 (2008).
[33] H. Eyring, J. Chem. Phys. **3**, 107 (1935).
[34] E. Wigner, Z. Phys. Chem. B **19**, 203 (1932).
[35] C. Eckart, Phys. Rev. **35**, 1303 (1930).
[36] A. González-Lafont, T. N. Truong, and D. G. Truhlar, J. Chem. Phys. **95**, 8875 (1991).
[37] D. G. Truhlar and A. Kupperman, J. Am. Chem. Soc. **93**, 1840 (1971).
[38] D. G. Truhlar and A. Kuppermann, J. Chem. Phys. **56**, 2232 (1972).
[39] D. G. Truhlar and B. C. Garrett, Annu. Rev. Phys. Chem. **35**, 159 (1984).
[40] A. Fernández-Ramos, J. Rodríguez-Otero, and M. A. Rios, J. Phys. Chem. A **102**, 2954 (1998).
[41] T. C. Allison and D. G. Truhlar, in *Modern Methods for Multidimensional Dynamics Computations in Chemistry*, edited by D. L. Thompson (World Scientific, Singapore, 1998), p. 618.
[42] D. G. Truhlar and B. C. Garrett, in *Hydrogen-Transfer Reactions*, edited by J. T. Hynes, J. P. Klinman, H.-H. Limbach, and R. L. Schowen (Wiley-VCH, Weinheim, Germany, 2007), Vol. **2**, p. 833.
[43] E. Wigner, J. Chem. Phys. **5**, 720 (1937).
[44] J. Horiuti, Bull. Chem. Soc. Jpn. **13**, 210 (1938).
[45] J. C. Keck, Adv. Chem. Phys. **13**, 85 (1967).
[46] B. C. Garrett and D. G. Truhlar, J. Chem. Phys. **70**, 1593 (1979).
[47] B. C. Garrett and D. G. Truhlar, Acc. Chem. Res. **13**, 440 (1980).
[48] P. Pechukas, Annu. Rev. Phys. Chem. **32**, 159 (1981).
[49] D. G. Truhlar, W. L. Hase, and J. T. Hynes, J. Phys. Chem. **87**, 2664 (1983).
[50] D. G. Truhlar, A. D. Isaacson, and B. C. Garrett, in *Theory of Chemical Reaction Dynamics*, edited by M. Baer (CRC, Boca Raton, Florida, 1985), Vol. **4**, p. 65.
[51] D. G. Truhlar, B. C. Garrett, and S. J. Klippenstein, J. Phys. Chem. **100**, 12771 (1996).
[52] B. C. Garrett and D. G. Truhlar, in *Theory and Applications of Computational Chemistry: The First Forty Years*, edited by C. E. Dykstra, G. Frenking, K. S. Kim, and G. E. Scuseria (Elsevier, Amsterdam, 2005), p. 67.
[53] A. Fernández-Ramos, A. Ellingson, B. C. Garrett, and D. G. Truhlar, Rev. Comput. Chem. **23**, 125 (2007).
[54] J. Pu, J. Gao, and D. G. Truhlar, Chem. Rev. **106**, 3140 (2006).
[55] J. M. L. Martin and G. de Oliveira, J. Chem. Phys. **111**, 1843 (1999).
[56] A. D. Boese and J. M. L. Martin, J. Chem. Phys. **121**, 3405 (2004).
[57] Y. Zhao, B. J. Lynch, and D. G. Truhlar, J. Phys. Chem. A **108**, 4786 (2004).
[58] J. Berkowitz, G. B. Ellison, and D. Gutman, J. Phys. Chem. **98**, 2744 (1994). Enthalpies of formation of the hydroxymethyl, methoxy, and hydrogen atom radicals were taken from Table X. The enthalpy of formation of methanol (–45.44 ±0.14 kcal/mol) was obtained from the NIST website.
[59] M. S. Gordon and D. G. Truhlar, J. Am. Chem. Soc. **108**, 5412 (1986).
[60] A. D. Becke, Phys. Rev. A **38**, 3098 (1988).
[61] A. D. Becke, J. Chem. Phys. **104**, 1040 (1996).
[62] Y. Zhao, B. J. Lynch, and D. G. Truhlar, J. Phys. Chem. A **108**, 2715 (2004).
[63] W. J. Hehre, R. Ditchfield, and J. A. Pople, J. Chem. Phys. **56**, 2257 (1972).
[64] B. J. Lynch, Y. Zhao, and D. Truhlar, J. Phys. Chem. A **108**, 1384 (2003).
[65] B. C. Garrett and D. G. Truhlar, J. Phys. Chem. **83**, 1052 (1979).
[66] A. González-Lafont, T. N. Truong, and D. G. Truhlar, J. Phys. Chem. **95**, 4618 (1991).
[67] K. Fukui, S. Kato, and H. Fujimoto, J. Am. Chem. Soc. **97**, 1 (1975).
[68] K. Fukui, Acc. Chem. Res. **14**, 363 (1981).
[69] M. A. Eliason and J. O. Hirschfelder, J. Chem. Phys. **30**, 1426 (1959).
[70] C. Steel and J. K. Laidler, J. Chem. Phys. **34**, 1827 (1961).
[71] M. Page and J. W. McIver, Jr., J. Chem. Phys. **88**, 922 (1988).
[72] Y.-Y. Chuang and D. G. Truhlar, J. Phys. Chem. A **102**, 242 (1998).
[73] E. Pollak and P. Pechukas, J. Am. Chem. Soc. **100**, 2984 (1978).
[74] A. Fernández-Ramos, B. Ellingson, R. Meana-Pañeda, J. Marques, and D. G. Truhlar, Theor. Chem. Acc. **118**, 813 (2007).
[75] B. C. Garrett, D. G. Truhlar, R. S. Grev, and A. W. Magnuson, J. Phys. Chem. **84**, 1730 (1980).
[76] Y.-P. Liu, D.-h. Lu, A. González-Lafont, D. G. Truhlar, and B. C. Garrett, J. Am. Chem. Soc. **115**, 7806 (1993).
[77] R. T. Skodje, D. G. Truhlar, and B. C. Garrett, J. Phys. Chem. **85**, 3019 (1981).
[78] R. T. Skodje, D. G. Truhlar, and B. C. Garrett, J. Chem. Phys. **77**, 5955 (1982).
[79] D.-h. Lu, T. N. Truong, V. S. Melissas, G. C. Lynch, Y.-P. Liu, B. C. Garrett, R. Steckler, A. D. Isaacson, S. N. Rai, G. C. Hancock, J. G. Lauderdale, T. Joseph, and D. G. Truhlar, Comput. Phys. Commun. **71**, 235 (1992).
[80] Y.-P. Liu, G. C. Lynch, T. N. Truong, D.-h. Lu, and D. G. Truhlar, J. Am. Chem. Soc. **115**, 2408 (1993).
[81] B. C. Garrett, D. G. Truhlar, A. F. Wagner, and T. H. Dunning, Jr., J. Chem. Phys. **78**, 4400 (1983).
[82] B. C. Garrett, N. Abusalbi, D. J. Kouri, and D. G. Truhlar, J. Chem. Phys. **83**, 2252 (1985).
[83] B. C. Garrett, T. Joseph, T. N. Truong, and D. G. Truhlar, Chem. Phys. **136**, 271 (1989).
[84] T. N. Truong, D.-h. Lu, G. C. Lynch, Y.-P. Liu, V. S. Melissas, J. J.P. Stewart, R. Steckler, B. C. Garrett, A. D. Isaacson, A. González-Lafont, S. N. Rai, G. C. Hancock, T. Joseph, and D. G. Truhlar, Comput. Phys. Commun. **75**, 143 (1993).
[85] A. Fernández-Ramos and D. G. Truhlar, J. Chem. Phys. **114**, 1491 (2001).
[86] A. Fernández-Ramos and D. G. Truhlar, J. Chem. Theory Comput. **1**, 1063 (2005).
[87] M. J. Frisch, G. W. Trucks, H. B. Schlegel *et al.*, GAUSSIAN03, *Revision B.04*, Gaussian, Inc., Pittsburgh, PA, 2003.
[88] J. C. Corchado, Y.-Y. Chuang, P. L. Fast, W.-P. Hu, Y.-P. Liu, G. C. Lynch, K. A. Nguyen, C. F. Jackels, A. F. Ramos, B. A. Ellingson, B. J. Lynch, J. Zheng, V. S. Melissas, J. Villa, I. Rossi, E. L. Coitiño, J. Pu, T. V. Albu, R. Steckler, B. C. Garrett, A. D. Isaacson, and D. G. Truhlar, POLYRATE 9.7, University of Minnesota, Minneapolis (2007).
[89] J. C. Corchado, Y.-Y. Chuang, E. L. Coitiño, Ellingson, J. Zheng, and D. G. Truhlar, GAUSSRATE 9.7, University of Minnesota, Minneapolis (2007).
[90] D. Lovy, WINDIG version 2.5 is a free data digitizer for Windows. http://www.unige.ch/sciences/chifi/cpb/windig.html.
[91] B. A. Ellingson, B. J. Lynch, S. L. Mielke, and D. G. Truhlar, J. Chem. Phys. **125**, 84305 (2006).
[92] K. S. Pitzer, J. Chem. Phys. **14**, 239 (1946).
[93] W. H. Gardiner, Jr., Acc. Chem. Res. **10**, 326 (1977).
[94] N. C. Blais, D. G. Truhlar, and B. G. Garrett, J. Chem. Phys. **85**, 1094 (1981).
[95] N. C. Blais, D. G. Truhlar, and B. C. Garrett, J. Chem. Phys. **76**, 2768 (1982).
[96] B. C. Garrett, D. G. Truhlar, J. M. Bowman, A. F. Wagner, D. Robie, S. Arepalli, N. Presser, and R. J. Gordon, J. Am. Chem. Soc. **108**, 3515 (1986).
[97] R. C. Tolman, J. Am. Chem. Soc. **42**, 2506 (1920).
[98] R. C. Tolman, *The Principles of Statistical Mechanics* (Claredon, Oxford, U.K., 1938).
[99] D. G. Truhlar, J. Chem. Ed. **55**, 309 (1978).
[100] D. G. Truhlar and A. Kohen, Proc. Natl. Acad. Sci. U.S.A. **98**, 848 (2001).
[101] L. Masgrau, A. González-Lafont, and J. M. Lluch, Theor. Chem. Acc. **110**, 352 (2003).
[102] J. Zheng and D. G. Truhlar, Phys. Chem. Chem. Phys. **12**, 7782 (2010).